Multiple laser shocking processing impacts on microstructure and mechanical property of high carbon steel

Yi XIONG [1,2*], Tian-tian HE [1], Yan LU [1], Han-sheng BAO[3],
Yong LI[3], Feng-zhang REN [1,2], Wei CAO[4,5],Alex A. VOLINSKY [6]

1.School of Materials Science and Engineering, Henan University of Science and Technology, Luoyang 471023, China

2. Collaborative Innovation Center of Nonferrous Metals, Luoyang 471023, China

3.Institute for Special Steels,Central Iron and Steel Research Institute, Beijin 100081,China

4.Nano and Molecular Systems Research Unit, University of Oulu, FIN-90014, Finland

5.School of Mechanical and Automotive Engineering, Anhui Polytechnic University, Wuhu 241000, China

6. Department of Mechanical Engineering, University of South Florida, Tampa FL 33620, USA.

ABSTRACT Multiple laser shocking processing (LSP) impacts on microstructures and mechanical properties were investigated through morphological determinations and hardness testing. Microscopic results show that without equal channel angular pressing (ECAP), the LSP treated lamellar pearlite was transferred to irregular ferrite matrix and incompletely broken cementite particles. With the ECAP, the LSP leads to refinements of the equiaxed ferritic grain in ultrafine-grained microduplex structure from 400 nm to 150 nm, and the completely spheroidized cementite particles from 150 nm to 100 nm. Consequentially, enhancements of mechanical properties were found in strength, microhardness and elongations of samples consisting of lamellar pearlite and ultrafine-grained microduplex structure. After the LSP, a mixture of quasi-cleavage and ductile fracture was formed, different from the typical quasi-cleavage fracture from the original lamellar pearlite, and the ductile fracture of the microduplex structure.

Keywords:

Laser shock processing

High carbon steel

Ultrafine-grained microduplex structure

Mechanical properties

1. Introduction

As a surface modification technique, the laser shock processing (LSP) is advanced in super-high strain rate deformation of the metal surface thanks to the intensive pulsed laser-induced plasma wave detonations [1]. The peak stress of the laser-induced shock wave is greater than material dynamic yield strength. Consequently, plastic deformation occurs on the metal surface with intensive stable dislocation structure, while hundreds of MPa of residual compressive stress is produced simultaneously in the metal surface layer. It can effectively improve strength [2], abrasive [3] and corrosion resistance [4], along with the fatigue life [5] of materials. Yet, the LSP has been widely used in advanced manufacturing. For instance, the LSP is employed in surface treatments for Ti alloys [6], magnesium alloys [7], aluminium alloys [8], coppers alloy [9], austenitic stainless steel [10] and carbon steel [11], etc. Despite these progresses, only microstructure response and properties change of the single-phased materials have been revealed under LSP super-high strain rate deformation. Though

*Corresponding author. Prof., Ph.D.
E-mail address: xy_hbdy@163.com (Y. Xiong).
Received ; Received in revised form ; Accepted
Available online

microstructure evolution and mechanical properties of microduplex structure were revealed during LSP [12,13], structural evolutions and property modifications in different structural states but from the same material remain unclear.

Understanding microstructure evolution and relevant properties variations in different original metal structures processed with the same deformation conditions allow establishing relations between microstructure response and strain-hardening effects. As a result, it provides basis for making further processing techniques and reasonably selecting materials. For these reasons, we investigated impacts of LSP on microstructure evolution and mechanical properties of high carbon steel with two different original structures of lamellar pearlite and ultrafine-grained microduplex structure. Mechanical properties have been improved after the laser treatment, along with microstructural modifications. It is hoped that this work can provide insightful experimental supports for the development and applications of the high carbon steel.

2. Materials and experimental procedure

The investigated steel ingot manufactured by the Fe-0.8C steel with the following chemical composition (in wt.%): 0.82C, 0.33Mn, 0.24Si, 0.011P, 0.012S and balance Fe. The samples were austenitizied at 1273 K for 30 min. A salt bath furnace was used to obtain the original structure with lamellar pearlite and the sample was treated at 873 K for 30 min. Other samples with ultrafine-grained microduplex structure were prepared by subsequent ECAP.

The samples used for ECAP were cut into cylinders with 8.3 mm diameters and 49 mm lengths. The intersecting angle between the two channels was 120° and the angle of the outer arc at the intersection was 30°. The 4-pass ECAP processing was performed at 923 K using the Bc route method. These ECAP specimens were rotated by 90° along the longitudinal axis of the specimen after each pass, in order to obtain a homogeneous microstructure. Before put in the entrance channel at the testing temperature, the specimen and the die were both coated with graphite and MoS_2 for lubrication. The detailed processing procedure can be found in our previous work [14]. Mini-tensile test specimens of lamellar pearlite and ultrafine-grained microduplex structure were sectioned along the longitudinal axis by wire cutting, as shown in Fig. 1a. Then the sample surface was polished and cleaned in deionized water. Subsequent LSP treatment was conducted on the gauge surface of the sample.

The LSP experiments were performed using a solid state Nd:glass phosphate laser with a wave length of 1.064 μm and a pulse duration of about 10 ns. 1 mm water layer was used as the transparent confining layer, while 100 μm aluminum tape as the absorbing layer. The spot diameter was 3 mm. The LSP impact time was 4 s and the laser energy was 6 J. The overlapping was 50%. The parameters used in LSP were shown in Ref. [15].其它实验参数详见表 1 所示。

Microstructure characterization was carried out using Field-emission scanning electron microscopy and transmission electron microscopy. For metallographic examination, samples were prepared by electrolytic etching using 4% Nital solution after LSP. For the TEM study, mechanically thinned 40 μm discs were prepared using ion polishing system. Operating voltage of TEM was set to 200 kV.

The mini-tensile test was conducted on the Instron 5948R micro material testing machine with a chuck moving velocity of 0.1 mm/min. The morphology of the fracture surfaces was observed using scanning electron microscopy, operated at 20 kV. Subsequently, microhardness of the laser processed

regions was measured by using HV-1000A Vickers microhardness tester. The load was 200 g and the holding time was 10 s. The laser processed regions with the interval distance of 0.2 mm along the longitudinal axis, as shown in Fig. 1b.

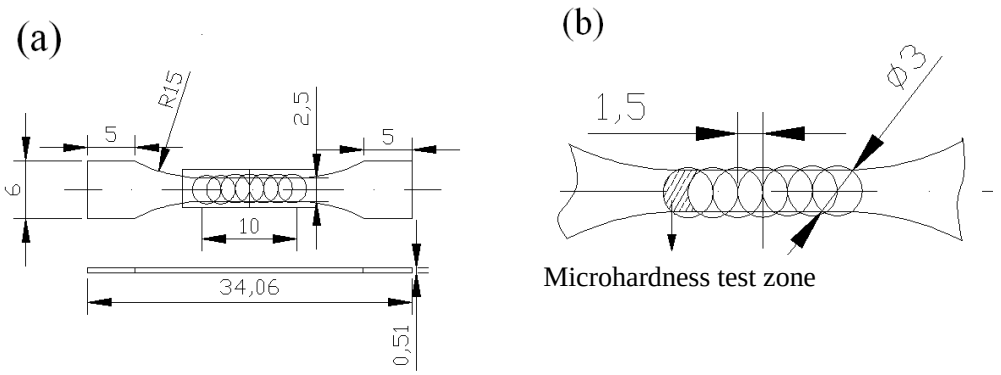

(a) dimensions of the tensile sample; (b) partially enlarged drawing of the treated area subjected to LSP.

Fig. 1. Dimensions of the mini-tensile sample.

Table 1 The processing parameters used in LSP.

Type	Value
Beam divergence of output (mmmrad)	≤2
Spot diameter (mm)	3
Pulse energy (J)	6
Impact times	4
Pulse width (ns)	10
Repetition-rate (Hz)	5
Laser wavelength (nm)	1064
Pulse to pulse energy stability (% rms)	<1.5%

3. Results and discussion

3.1. Microstructure evolution of high carbon steel before LSP

Fig. 2 shows the SEM and TEM images of the high carbon steel with different original structures before LSP treatment. In Fig. 2(a), Fe-0.8C steel shows full lamellar pearlitic structure after isothermal treatment at 600 °C. After four ECAP passes, the original pearlitic lamellae disappeared totally, but traces of arrangement direction of the initial cementite lamellae can be observed. To accommodate the shear deformation of ECAP, the cementite lamella are severely bent and kinked. Meanwhile, spheroidization of the cementite occurred and increased with deformation, as observed in Fig. 2(b). From TEM micrographs in Fig. 2(c,d), the lamellae spacing of the cementite is determined to ~ 150 nm, and thickness to ~30 nm (Fig. 2(c)). Fig. 2d shows the ultrafine-grained microduplex structure with sub-micron grain size after four ECAP passes. The sizes of equiaxed ferrite grains and the cementite particles are about 400 nm and 150 nm, respectively. During the warm deformation, the equiaxial process of ferrite coordinates with the spheroidization of the cementite lamellae [16]. During the initial stage of plastic deformation, high density dislocation lines develop in the ferrite grains. The

dislocation tangles and dense dislocation cells are formed due to pile-up of the dislocation lines [17,18]. Some sub-grains of the dislocated cells become sharper following strain increase. Then high angle grain boundaries develop due to the continuous dynamic recrystallization in the sub-grain boundaries, which refines the ferrite grains [15,19]. Meanwhile, the diffusion of Fe and C atoms is speeded up due to the dislocation tangles and sub-grain boundaries, accelerating cementite spheroidized process.

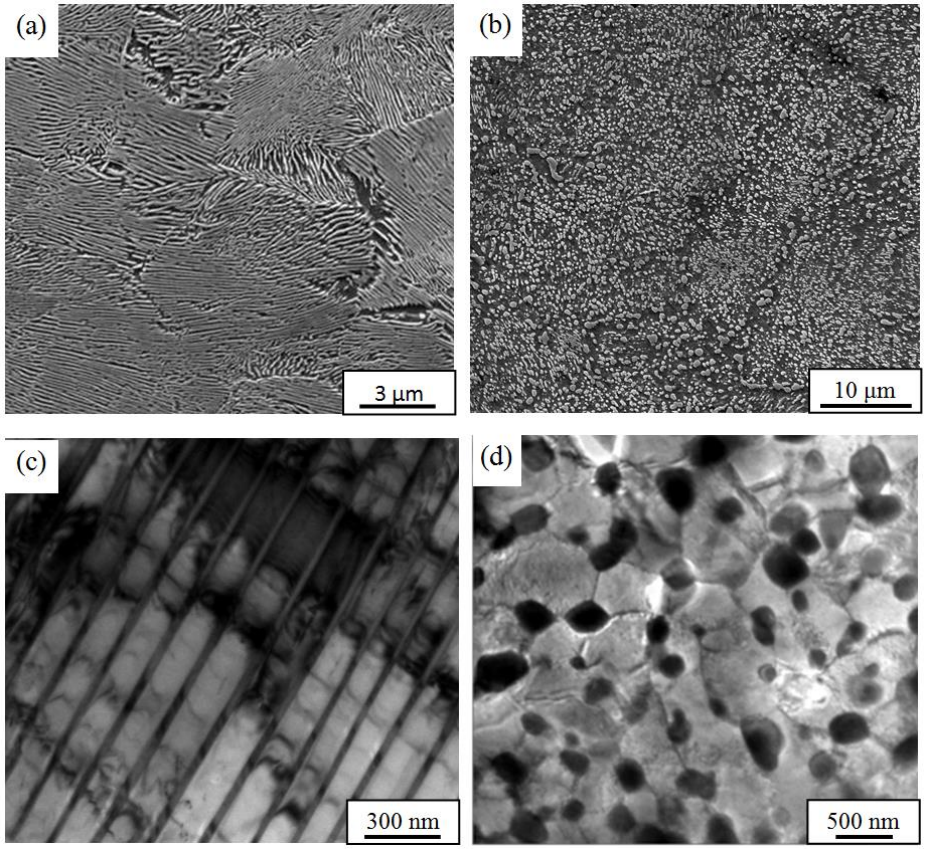

(a) SEM morphology of lamellar pearlite; (b) SEM morphology of ultrafine-grained microduplex structure; (c) TEM morphology of lamellar pearlite; (d) TEM morphology of ultrafine-grained microduplex structure.

Fig. 2. Micrographs of the high carbon steel before LSP.

3.2 Microstructure evolution of high carbon steel after LSP

Fig. 3 shows microscopic images of the high-carbon steel with two different original microstructures after LSP. SEM figures in Fig. 3a and b show that the lamellar pearlitic structure is kinked, bent and fractured at the same time along with the broken of the cementite lamellae. However, the configuration direction is still kept in Fig. 3(a). After multiple LSP treatments, the cementite of ultrafine-grained microduplex structure is completely fractured into granules, and particle diameter decreases from 150 nm to 100 nm (Fig. 3(b)). The corresponding TEM micrographs are shown in Fig. 3(c,d). After LSP of the lamellar pearlitic structure, more dislocations are formed and dislocation density obviously increases in the ferrite matrix. The parallel lamellar pearlites are broken into some segments, and dislocation activities simultaneously lead to the formation of dislocation lines and

dislocation tangles in the ferrite grains. With increasing number of laser shocks, the broken lamellar pearlites are further fragmented to bitty pearlites. These dislocation configurations gradually developed to subdivision of ferrite grains by forming individual primarily separated dislocation cells. Consequently, the ferrite matrix was refined, and represented by ~ 700 nm irregular ferrite grains. However, the cementite lamellae are insufficient broken into bitty cementite, and most of them are on the grain boundaries, little completely broken cementite particles located in the ferrite grains (Fig. 3(c)). In contrast, after LSP treatment for the ultrafine-grained microduplex structure, as seen in Fig. 3d, the ferrite grain is further refined and the fragmentation of cementite granules is more completely. The average grain size of equiaxed ferrite grains and completely fractured cementite particles are further refined to about 150 nm and 100 nm (Fig. 3(d)). This is in line with the observation as shown in Ref. [20], where grains in the surface layer of ANSI 304 stainless steel subjected to multiple LSP impacts were extremely refined down to ~ 50-200 nm at the top surface. Also, Lamiale et al [21] studied the grain size change of the ultrafine grain materials after high strain rate deformation by using the finite elements software based on dislocation viscoplastic model. Therein, the grain size of the ultrafine grain materials can be further refined under high strain rate deformation. Our results agree well with these previously reported.

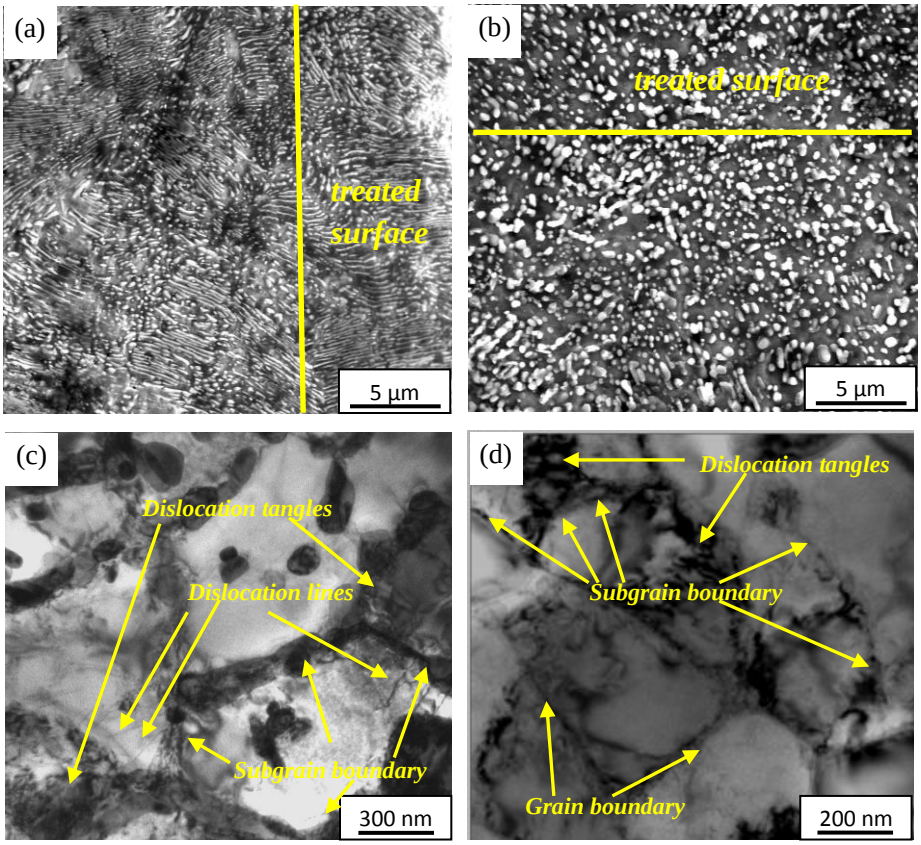

(a) SEM morphology of lamellar pearlite; (b) SEM morphology of ultrafine-grained microduplex structure; (c) TEM morphology of lamellar pearlite; (d) TEM morphology of ultrafine-grained microduplex structure.

Fig. 3. Micrographs of the high carbon steel after LSP.

3.3 Mechanical properties and microhardness of high carbon steel after LSP

The engineering stress-strain curves from the mini-tensile test of the high-carbon steel with different original structures before and after LSP are shown in Fig. 4. The LSP enhances strength and elongation of the high-carbon steel with different original structures. The ultimate tensile strengths increase from 867±5 MPa (lamellar pearlite structure) and 819±5 MPa (ultrafine-grained microduplex structure) to 920±5 MPa and 871±5 MPa, respectively. The corresponding yield strengths increase from 477±5 MPa and 662±5 MPa to 520±5 MPa and 685±5 MPa, respectively. Meanwhile, after LSP the elongation significantly increased from 5% and 18% to 10% and 20% for the lamellar pearlite structure and ultrafine-grained structure, respectively. The local plastic deformation after LSP leads to the generation of the compressive residual stresses near the specimen surface. Indeed, here the high intensity short pulsed laser beam bombards and vaporizes opaque sacrificial coating on the metal work piece. Vapor and plasma absorb the incident laser energy and violently explode against the metal surface. A portion of the energy propagates as a shock wave into the metal. When the shock wave pressure exceeds metal yield strength, metal deforms plastically and a large amount of dislocations turns out. Thus, a layer with residual compressive stress forms on its surface [22]. The fatigue performance can be improved by the compressive residual stresses [23]. The presence of compressive residual stresses inhibits the fatigue crack initiation and growth, and prolongs the crack propagation life. Consequentially, after LSP, mechanical properties of the high-carbon steel with different original structures are enhanced by the compressive stresses at the surface.

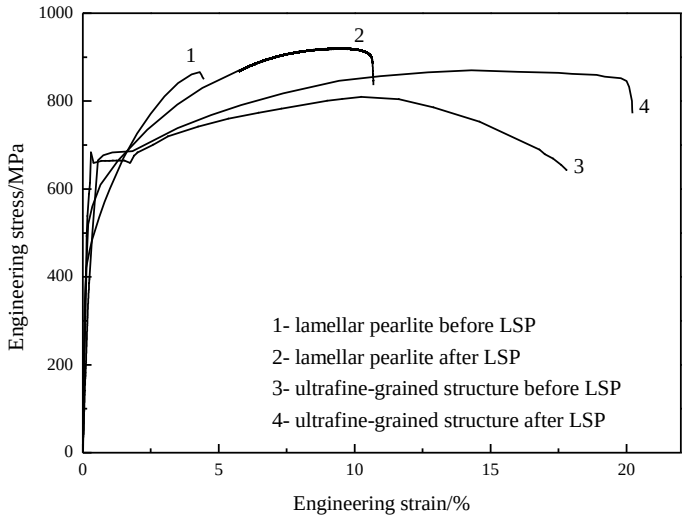

Fig. 4. Engineering stress-strain curves from the mini-tensile test of the high-carbon steel with different original structures before and after LSP.

Microhardness of the high-carbon steel with different original structures after LSP is shown in Fig. 5. Surface hardness obviously increases after LSP for the samples with two different original structures. Increase of the hardness at the center of the laser spot is much higher than regions farther apart from the spot. This is because the stress induced by the shock wave has a Gaussian distribution due to the intrinsic character of the laser pulse energy. The microhardness of ultrafine-grained microduplex structure increased by 27% from 296 HV to 376 HV at the impact center. The percentage

is about 2 times of the increase of initial lamellar pearlites structure, say 14% from 302 HV to 342 HV. After LSP of the lamellar pearlitic structure, there is severe plastic deformation in the metal surface, resulting in the increase of the dislocation density, and formations of dislocation cells and pinning of dislocations. Meanwhile, large stress concentration emerged in the local area, leading to obvious work-hardening. Furthermore, the ferrite grain is refined to 700 nm (Fig. 3c). As a result, the hardness is evidently improved. At the same time the cementite lamellae are kinked, bent, fractured and broken into granules constantly in the lamellar pearlite structure, decreasing microhardness. The microhardness at the center of the laser spot of the lamellar pearlite increases slowly under the combined interactions of work-hardening, grain refinement and the fragmentation of cementite. After LSP of the ultrafine-grained microduplex structure, the ferrite is further refined (Fig. 3d). The fragmentation of cementite granules is more completely, and their size is further decreased. Meanwhile, partial dissolution of the cementite occurs, leading to supersaturated carbon atoms. This phenomenon was proved by our previous work [24]. Microhardness in the impact center of ultrafine-grained microduplex structure increases remarkably, compared to the one of lamellar pearlite structure. This is mainly due to grain refinement and solution strengthening. However, the hardness and the ultimate tensile strength do not follow the basic law where hardness is one-third of the ultimate tensile strength. This is mainly because after LSP, a gradient structure was formed from the sample surface to the core [20]. Thus, the ultimate tensile strength represents the overall performance of the samples, while the hardness is tested at the sample surface.

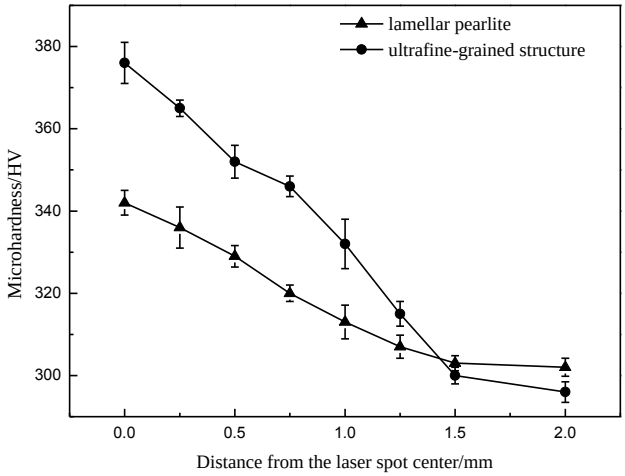

Fig. 5. Microhardness of the high carbon steel with different original structures after LSP.

3.4 Fracture surface morphology

The fracture surface morphology of the high-carbon steel with two different original microstructures before and after LSP is shown in Fig. 6. Before LSP, the fracture surfaces of the original lamellar pearlite structure and ultrafine-grained microduplex structure are quasi-cleavage fracture and ductile fracture, respectively. In Fig. 6(a), a typical river-like pattern can be observed and a small amount of microcracks and tear ridges exhist around the river pattern. The fracture surface of the sample is smooth, and decorated with dimples varying in sizes and depths. The average size of a few large and deep dimples is about 8 μm, while a large number of small and shallow dimples are

distributed uniformly at an average size of ~1 μm (see Fig. 6(b)). After LSP, the fracture morphology shows a mixture of quasi-cleavage and ductile fracture. The quasi-cleavage fracture occurs both at the sample surface (ultrafine-grained microduplex structure) and inside the sample (lamellar pearlite structure), while ductile fractures exist inside of the sample (ultrafine-grained microduplex structure) and at the sample surface (lamellar pearlite structure). This is mainly due to the severe plastic deformation (SPD) layer with a certain depth (about 50 μm) at the sample surface after LSP, as shown in Fig. 6(c,d). For the lamellar pearlite structure, cementite lamellar fracture in the plastic deformation layer improves the plastic deformation capacity of the lamellar pearlite structure. The fracture surface shows ductile fracture. For the ultrafine-grained microduplex structure, work hardening occurs in the plastic deformation layer, which results in the quasi-cleavage fracture. Thus, the fracture surface of the two different original microstructure of the high-carbon steel after LSP is a mixture of quasi-cleavage and ductile fracture. This is consistent with the results of LY2 alloy after multiple LSP by Lu et al [25]. From Fig. 6, it can be also seen that the gradient structure forms in the high carbon steel after LSP. With the increase of the distance to the treated surface, the microstructure evolves from dislocation lines (inside the sample) to dislocation tangles and dislocation walls (sub-surface), and to subgrains and ultrafine grains (outer surface). This may be attributed to decreases of the strain and stress following the increase of distance to the treated surface [15].

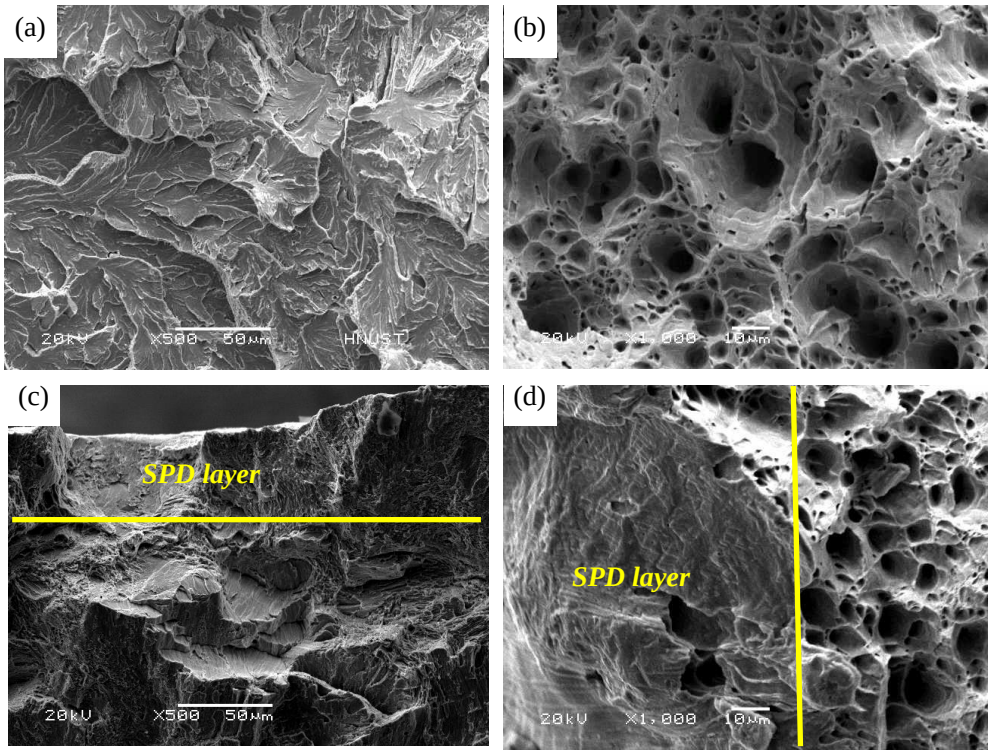

(a) before LSP of lamellar pearlite; (b) before LSP of ultrafine-grained microduplex structure; (c) after LSP of lamellar pearlite; (d) after LSP of ultrafine-grained microduplex structure.

Fig. 6. Fracture surfaces morphology of the high-carbon steel with two different initial microstructures before and after LSP.

4. Conclusions

In conclusion, we carried out a comprehensive study of laser shock processing impacts on high carbon steel mechanical properties and microstructure. The work is concluded as following:

(1) The microstructure of high-carbon steel with different original structures was effectively refined by multiple LSP. The lamellar pearlite changed into irregular ferrite matrix and incompletely broken cementite particle after LSP. The ferrite grain size is 700 nm. Equiaxed ferritic grain and completely spheroidized cementite particle in ultrafine-grained microduplex structure were further refined from 400 nm and 150 nm to about 150 nm and 100 nm grain size, respectively.

(2) Mechanical properties of the high-carbon steel with different original microstructure are improved after multiple LSP. The microhardness of ultrafine-grained microduplex structure increased 27%, which is 2 times higher than the initial lamellar pearlites structure of 14%. Meanwhile, after LSP the elongation of the lamellar pearlite sharply increased.

(3) The fracture surfaces morphology changes from typical quasi-cleavage fracture (lamellar pearlite) and ductile fracture (ultrafine-grained microduplex structure) to a mixture of quasi-cleavage and ductile fracture after LSP.

Acknowledgment

This work was supported by the NSFC (50801021, 51201061), and by Program for Science, Technology Innovation Talents in Universities of the Henan Province (17HASTIT026), the Science and Technology Project of the Henan Province (152102210077), International Scientific and Technological Cooperation Project from Science and Technology Department of Henan Province(172102410032), Education Department of the Henan Province (16A430005) and the Science and Technology Innovation Team of the Henan University of Science and Technology (2015XTD006).

References

[1] C.S. Montross, T. Wei, L. Ye, G. Clark, Y.W. Mai, Int. J.Fatigue. 24 (2002) 1021-1036.

[2] B.P. Fairand, B.A. Wilcox, W.J. Gallagher, D.N. Williams, J. Appl. Phys. 43 (1972) 3893-3895.

[3] J.Z. Lu, K.Y. Luo, F.Z. Dai, J.W. Zhong, L.Z. Xu, C.J. Yang, L.Zhang, Q.W. Wang, J.S. Zhong, D.K. Yang, Y.K. Zhang, Mater. Sci. Eng. A 536 (2012) 57-63.

[4] H. Lim, P. Kim, H. Jeong, S. Jeong, J. Mater. Process. Tech. 212 (2012) 1347-1354.

[5] X.F. Nie, W.F. He, S.L. Zang, X.D. Wang, J. Zhao, Surf. Coat. Tech. 253 (2014) 68-75.

[6] J.Z. Lu, L.J. Wu, G.F. Sun, K.Y. Luo, Y.K. Zhang, J. Cai, C.Y. Cui, X.M. Luo, Acta.Mater. 127 (2017) 252-266.

[7] M.Z. Ge, J.Y. Xiang, J. Alloy. Compd. 680 (2016) 544-552.

[8] S. Huang, J.Z. Zhou, J. Sheng, K.Y. Luo, J.Z. Lu, Z.C. Xu, X.K. Meng, L. Dai, L.D. Zuo, H.Y. Ruan, H.S. Chen, Int. J. Fatigue 47 (2013) 292-299.

[9] J. Cai, S. Shekhar, J. Wang, M.R. Shankar, Scripta Mater. 60 (2009) 599-602.

[10] J.Z. Lu, J.S. Zhong, K.Y. Luo, L. Zhang, H. Qi, M. Luo, X.J. Xu, J.Z. Zhou, Surf. Coat. Tech. 221 (2013) 88-93.

[11] C. Ye, S. Suslov, B. J. Kim, E.A. Stach, G.J. Cheng, Acta. Mater. 59 (2011) 1014-1025.

[12] C.R. González，C.F. Martinez, G.G. Rosas, J.L. Ocâna, M. Morales, J.A. Porro, Mater. Sci. Eng. A 528 (2011) 914-919.

[13] X.M. Luo, G.Z. Zhao, Y.K. Zhang, K.M. Chen, K.Y. Luo, X.D. Ren, Acta.Metall.Sin. 48 (2012) 1116-1122 (in Chinese).

[14] T.T. He, Y. Xiong, F.Z. Ren, Z.Q. Guo, A.A. Volinsky, Mater. Sci. Eng. A 535 (2012) 306-310.

[15] J.Z. Lu, K.Y. Luo, Y.K. Zhang, C.Y. Cui, G.F. Sun, J.Z. Zhou, L. Zhang, J. You, K.M. Chen, J.W. Zhong, Acta Mater. 58 (2010) 3984-3994.

[16] E. Werner, Acta Mater. 37 (1989) 2047-2053.

[17] R. Kaspar, W. Kapellner, C. Lang, Steel Res. 59 (1988) 492-498.

[18] E.A. Chojnowski, W.J.M. Tegart, Metal Sci. J. 2 (1968) 14-18.

[19] J.Z. Lu, J.W. Zhong, K.Y. Luo, L. Zhang, F.Z. Dai, K.M. Chen, Q.W. Wang, J.S. Zhong, Y.K. Zhang, Mater. Sci. Eng. A 528 (2011) 6128-6133.

[20] J.Z. Lu, K.Y. Luo, Y.K. Zhang, G.F. Sun, Y.Y. Gu, J.Z. Zhou, X.D. Ren, X.C. Zhang, L.F. Zhang, K.M. Chen, C.Y. Cui, Y.F. Jiang, A.X. Feng, L. Zhang, Acta Mater. 58 (2010) 5354-5362.

[21] V. Lemiale, Y. Estrin, H.S. Kim, R.O. Donnell, Comput. Mater. Sci. 48 (2010) 124-132.

[22] Z. Zhou, S. Bhamare, G. Ramakrishnan, S.R. Mannava, K. Langer, Y.H. Wen, D. Qian, V.K. Vasudevan, Surf. Coat. Tech. 206 (2012) 4619-4627.

[23] X.D. Ren, Q.B. Zhan, H.M. Yang, F.Z. Dai, C.Y. Cui, G.F. Sun, L. Ruan, Mater. Design 44 (2013) 149-154.

[24] Y. Xiong, T.T. He, F.Z. Ren, P.Y. Li, L.F. Chen, A. A.Volinsky, J. Iron. Steel. Res. Int. 22 (2015) 55-59.

[25] J.Z. Lu, K.Y. Luo, Y.K. Zhang, J.Z. Zhou, X.G. Cui, L. Zhang, J.W. Zhong., Mater. Sci. Eng. A 528 (2010) 730-735.